Microchimica Acta (2019) 186:856
https://doi.org/10.1007/s00604-019-3929-0

ORIGINAL PAPER

A porous carbon nitride modified with cobalt phosphide as an efficient visible-light harvesting nanocomposite for photoelectrochemical enzymatic sensing of glucose

Dong Liang[1] · Junjun Luo[1] · Yaliang Huang[1] · Xiang Liang[1] · Xiaoqing Qiu[1] · Jianxiu Wang[1] · Minghui Yang[1]

Received: 13 June 2019 / Accepted: 12 October 2019

Abstract
A porous carbon nitride (PCN) modified with cobalt phosphides (CoP) was synthesized. In this nanocomposite, the CoP (in different weight fractions) serves (a) as the electron acceptor to accelerate the photoinduced charge separation, and (b) as the photosensitizer to increase the photoelectrochemical (PEC) response to visible light. Dissolved oxygen acts as the electron acceptor to generate PEC current. If glucose oxidase (GOx) catalyzes the oxidation of glucose, dissolved oxygen is consumed. This leads to the suppression of photocurrent. The photocathode biosensor has a linear response in the 0.05 to 0.7 mM glucose concentration range and a 1.1 μM limit of detection.

Keywords CoP · Electron acceptor · Visible light · Oxygen · Photocathode

Introduction

Photoelectrochemical (PEC) detection has tremendous advantages in biosensor design such as easy to miniaturize, high sensitivity, cost-effective and low background signal [1, 2, 3–5]. PEC biosensors are based on the photocurrent change though the biological interactions between recognition elements and their corresponding analytical targets [6]. In PEC detection, the photoelectroactive material acts not just as the energy transducer layer, but as the suitable support for immobilization of the recognition elements [7]. Therefore, it is highly important to synthesize good performance photoelectroactive materials.

TiO_2 proved to be a good material for PEC biosensors because of its biocompatibility, photoelectric activity, good stability, environmental safety, and low cost [8, 9]. However, the practical applications of TiO_2 are restricted by its large band gap (~3.2 eV), which absorb only the ultraviolet light (<387 nm) [10]. Beside the poor utilization of light energy, the biological recognition elements immobilized on TiO_2 will be easily denatured under the ultraviolet light illumination [11]. As a result, the synthesis of photoelectroactive materials with high visible-light activity has attracted significant interest, including inorganic semiconductors ($BiVO_4$, BiOI) and organic semiconductors (such as tris-(bipyridyl)ruthenium complex) [12–14]. Especially, the metal-free semiconductor, namely graphitic carbon nitride (g-C_3N_4), is especially protruding in the design of PEC biosensors, due to its fascinating conjugated structure, visible-light response, and earth-abundant nature [15]. Liu et al. used the g-C_3N_4/TiO_2 as a scaffold to design photoelectrochemical enzyme biosensor with wide linear range and low glucose detection limit [16]. So, coupling g-C_3N_4 with earth-abundant co-catalyst can accelerate the photocharge separation, further improving the PEC properties of materials.

Transition metal phosphide has been extensively studied because of its good stability as compared to metal chalcogenides, and better conductivity as compared to metal oxides [17]. Among these phosphide catalyst, CoP with narrow E_g (~1.7 eV) possesses outstanding PEC efficiency in visible-light region [18]. Herein, we used CoP nanoparticles as the

Electronic supplementary material The online version of this article (https://doi.org/10.1007/s00604-019-3929-0) contains supplementary material, which is available to authorized users.

✉ Minghui Yang
yangminghui@csu.edu.cn

[1] College of Chemistry and Chemical Engineering, Central South University, Changsha, Hunan 410083, People's Republic of China

Published online: 29 November 2019

noble-metal-free co-catalyst for porous graphitic carbon nitride (PCN, CoP/PCN) to enhance the visible-light activity of the nanocomposite.

Glucose (Glu) is the major energy source in a wide variety of biological process [19, 20]. To date, various types of glucose sensors including optical and electrochemical sensors have been reported. These sensors were typically focused on the detection of high concentration of Glu in diagnosing system (2–30 mM) [16, 21, 22]. However, either elevated or lowered glucose level in body will affect cell functions. The concentration of glucose in body fluids can be down to several μM [23]. Here, CoP/PCN was utilized as PEC material and immobilization support for enzyme glucose oxidase (GO_x) to construct PEC biosensor for detection of low level of Glu. The CoP/PCN photocathode biosensors exhibited satisfactory detection performance with linear range from 0.05 to 0.7 mM and limit of detection down to 1.1 μM.

Experimental section

Material and reagents

$Co(NO_3)_2{\cdot}6H_2O$, sodium citrate, NaH_2PO_2, KH_2PO_4 and K_2HPO_4 were purchased from Aladdin Ltd. (Shanghai, China, https://www.aladdin-e.com/). Melamine was obtained from Sangon Biotech Co., Ltd. (Shanghai, China, https://www.sangon.com/). Glucose oxidase (GO_x) and Nafion were purchased from Sigma Aldrich (https://www.sigmaaldrich.com/). All solutions were prepared in MilliQ water.

Apparatus

The morphologies of the materials were characterized by scanning electron microscopy (SEM) on a JEOL JSM-6700 microscope, and transmission electron microscopy (TEM) on a Philips-FEI Tecnai G2 F20 microscope. The crystalline structure of the materials was studied by X-ray diffraction (XRD) on a D/MAX2500 V diffractometer using Cu Kα radiation. X-ray photoelectron spectroscopy (XPS) data were recorded by an ESCA Lab220i-XL electron spectrometer from VG Scientific using 300 W Al Kα radiation. UV-vis diffuse reflection spectroscopy (DRS) was performed on a TU-1901 2450 spectrophotometer (Persee, China), in which $BaSO_4$ was used as a reference standard.

Preparation of g-C_3N_4 and porous carbon nitride (PCN)

Bulk g-C_3N_4 was synthesized by thermal treatment of melamine for 4 h at 550 °C with temperature increased at heating rate of 5 °C·min^{-1}. After cooling, the yellow agglomerates were milled into powder in an agate mortar to obtain g-C_3N_4 (noted as CN). The PCN was synthesized through the alkaline hydrothermal treatment of g-C_3N_4 according to the following procedures. In detail, g-C_3N_4 (0.8 g) was added into 70 mL of NaOH solution (0.12 M) with continuous stirring for 30 min. Then, the mixture was transferred to a 100 mL Teflon-sealed autoclave and maintained at 120 °C for 18 h. The resulting products were washed with ethanol and distilled water, and dried in an oven at 80 °C overnight.

Preparation of CoP/PCNs

The CoP/PCN nanocomposites were prepared via a thermal phosphidation reaction using $Co(OH)_2$ and PCN as precursors. In a typical process, $Co(NO_3)_2{\cdot}6H_2O$ (100 mg) and sodium citrate (25 mg) were dissolved in 50 mL aqueous solution. The PCNs, with different weight percentage (0.3, 0.5, 0.8, 1, 2, 5, 10 and 20 wt% of CoP) was adding into the mixture under vigorous stirring for 30 min. Then, excess NaOH solution (0.5 M) was added to the mixture dropwise. The suspensions were centrifuged, washed by ethanol and distilled water, and then dried at vacuum oven to obtain ($Co(OH)_2$/PCN). Subsequently, the $Co(OH)_2$/PCN and NaH_2PO_2 solid were grounded in a mortar to form a uniform mixture (The molar ratio for Co to P is 1:5). The mixture was heated in Ar atmosphere at 300 °C for 1 h with a heating rate of 2 °C·min^{-1}. The CoP/PCNs were washed by water and ethanol three times and dried at vacuum oven.

Preparation of the PEC glucose biosensor

For preparation of the biosensor, 20 mg of CoP/PCN was dispersed into 1 mL solution containing 300 μL of aqueous GO_x solution (2 mg·mL^{-1}). Then, 50 μL of Nafion (5% *w*/w) was added into the mixture and agitated at 4 °C for 4 h. Finally, 20 μL of this mixture was dropped onto cleaned glassy carbon electrode (GCE, diameter, 5 mm) and dried at 4 °C for 8 h. For comparison, PCN and CoP/PCN modified electrodes were also prepared using the same procedure without GO_x.

PEC measurement

A 300 W Xe lamp equipped with optical filter (>420 nm) was served as the visible light irradiation source. The PEC measurement was performed on a CHI660E electrochemical workstation with a three-electrode system, consisting of a GCE working electrode, a Pt wire auxiliary electrode and an Ag/AgCl reference electrode. In PEC experiments, PEC response of the biosensor was first recorded in phosphate buffered solution (PB, 10 mM, pH 7.4, 30 mL) at −0.2 V (vs. Ag/AgCl) under visible light irradiation. After that, the electrode was immersed in 30 mL of PB solution containing different

concentrations of glucose and incubated at 37 °C for 30 min. Finally, the photocurrent was also recorded in the incubated PB solution under light irradiation at −0.2 V (vs. Ag/AgCl).

Furthermore, the GO_x/CoP/PCN modified electrodes was used to determine glucose concentration in human serum sample. Human serum samples were received from the Second Xiangya Hospital, and the level of glucose was measured to be 4.6 mM by the hospital. The concentration of glucose was also determined by our sensor and then, the recovery of glucose was tested by addition of standard glucose to the serum samples.

Results and discussion

Choice of materials

Compared to the metal oxide semiconductor, polymeric carbon nitride (CN) possesses visible-light bandgap (2.7 eV), which can achieve more efficient utilization of the sunlight [24]. Meanwhile, porous carbon nitride (PCN) is also regarded as a promising substrate material, which can be ascribed to the two-dimensional conjugate structure and high specific surface area. CoP as a noble-metal-free cocatalyst possess a narrow bandgap (~1.7 eV), which also act as a promising visible-light catalyst. As a result, coupling PCN with CoP can accelerate the photocharge separation and form an effective photocatalyst because of their higher stability as compared to quantum dot, and better conductivity as compared to metal oxides.

Material characterization

The schematic representation for the synthesis of CoP/PCN nanocomposites is illustrated in Fig. 1a. Bulk g-C_3N_4 was first treated by alkaline hydrothermal treatment to form PCN. Then, $Co(OH)_2$ was loaded onto the surface of PCN. Finally, $Co(OH)_2$ loaded on the surface of PCN were in situ phosphated to CoP through thermal treatment.

The crystal structure of the materials was characterized by XRD (Fig. 1b). The g-C_3N_4 exhibits the characteristic diffraction peaks at 13.1° and 27.4°, corresponding to the (100) and (002) planes (JCPDS No. 87–1526) [25]. For PCN, the (002) peak is strengthened and broadened due to lower grain size and higher crystallinity of PCN [26]. As for the CoP/PCN nanocomposites (2 wt% of CoP), the characteristic diffraction peaks of g-C_3N_4 and CoP are observed, indicating that CoP is successfully loaded onto PCN [27]. The relatively weak peaks of CoP can be attributed to the low CoP content. Scanning electron microscope (SEM) and energy dispersive spectroscopy (EDS) measurements were further performed to reveal the morphology and element of the materials, as shown in Fig. S1.

The composition and chemical state of elements of CoP/PCN were studied by XPS spectra. The full XPS spectrum of CoP/PCN further evidences the presence of the C, N, Co and P elements (Fig. S2). As shown in Fig. 2a, the XPS spectra of C 1 s of CoP/PCN can be divided into two peaks located at 284.8 and 287.8 eV, being assigned to C-C and N-C=N bonds, respectively [28]. The high resolution N 1 s spectrum of CoP/PCN is also separated into three peaks. The dominant peak at 398.3 eV is ascribed to C=N-C, and the peak located at 398.9 eV and 400.3 eV are attributed to N-C_3 and C-N-H [29]. As shown in Fig. 2, the characteristic peaks of Co 2p 3/2 (780.1 eV) and P 2p3/2 (132.8 eV) in the high-resolution XPS spectra confirm the phase of CoP [18].

Furthermore, the microstructure of the CoP/PCN nanocomposite was characterized by TEM. As shown in Fig. S3a, the PCN exhibits the porous structure, which was attributed to the exfoliation of g-C_3N_4 during the alkali-based hydrothermal treatment. The porous structure of PCN indicates high specific surface area, which is beneficial for the PEC performance of CoP/PCN nanocomposite. As for CoP in CoP/PCN nanocomposite, Fig. 3a and Fig. S3c shows CoP nanoparticles (~8–12 nm) are anchored on the surface of PCN nanosheets. The HRTEM image of the CoP/PCN is shown in Fig. 3b. By measuring the lattice fringes, the lattice spacing of 2.31 Å is related to the (201) diffraction plane of CoP [27]. The priority for the good PEC performance of the photoactive material is its light absorption efficiency [30]. As shown in Fig. S4, for the CoP/PCN, UV–vis light absorption expands to the entire wavelength. Therefore, the loading CoP on PCN can obviously strengthen the absorption efficiency of CoP/PCN in the visible-light region.

PEC mechanism and analytical performance of CoP/PCN biosensor for glucose

Different experimental conditions, such as the effect of CoP loading, Nafion loading and applied potential were investigated to obtain the optimum biosensor performance [31]. As shown in Fig. S5, the experimental conditions were found to give best results: (a) Optimal CoP percentage: 2%; (b) Optimal Nafion concentration: 0.7%; (c) Optimal applied potential: −0.2 V vs. Ag/AgCl.

Based on the experimental conditions, photocurrent responses of g-C_3N_4, PCN, CoP/PCN and GO_x/CoP/PCN were characterized to prove the enhanced photocurrent response of CoP/PCN (Fig. 4a). As for g-C_3N_4, the lowest photocurrent response is observed. After the activation by the alkaline hydrothermal treatment, the photocurrent of PCN is obviously enhanced. Notably, a further ~5-fold increase of photocurrent is observed for the CoP/PCN modified electrodes compared with PCN, which can be attributed to the properties of CoP/PCN including strong visible light absorption and low charge recombination [27, 32]. As for the GO_x/CoP/PCN modified

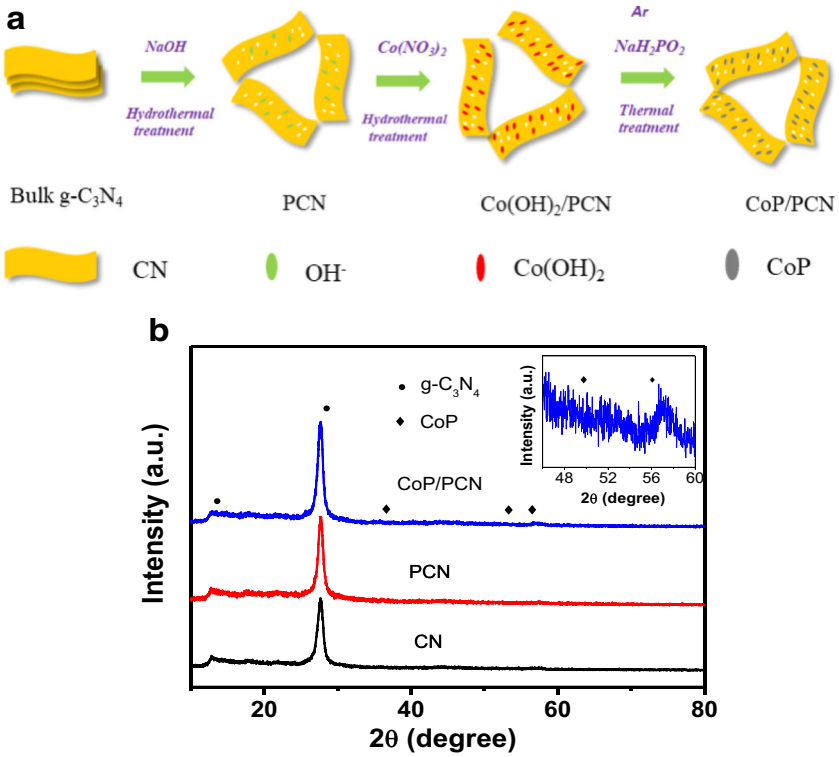

Fig. 1 **a** The formation principle of CoP/PCN. **b** XRD patterns of CN, PCN, CoP/PCN (2 wt% of CoP)

electrode, considering the insulating properties of the anchored enzyme GO_x, a moderate decline of the photocurrent is recorded. Furthermore, the charge separation efficiency of materials was also examined by EIS measurements [33]. As shown in Fig. 4b, the smaller diameter of the Nyquist plots for CoP/PCN demonstrates the decreased electron transfer resistance compared with g-C_3N_4 or PCN, which may result in enhanced PEC response.

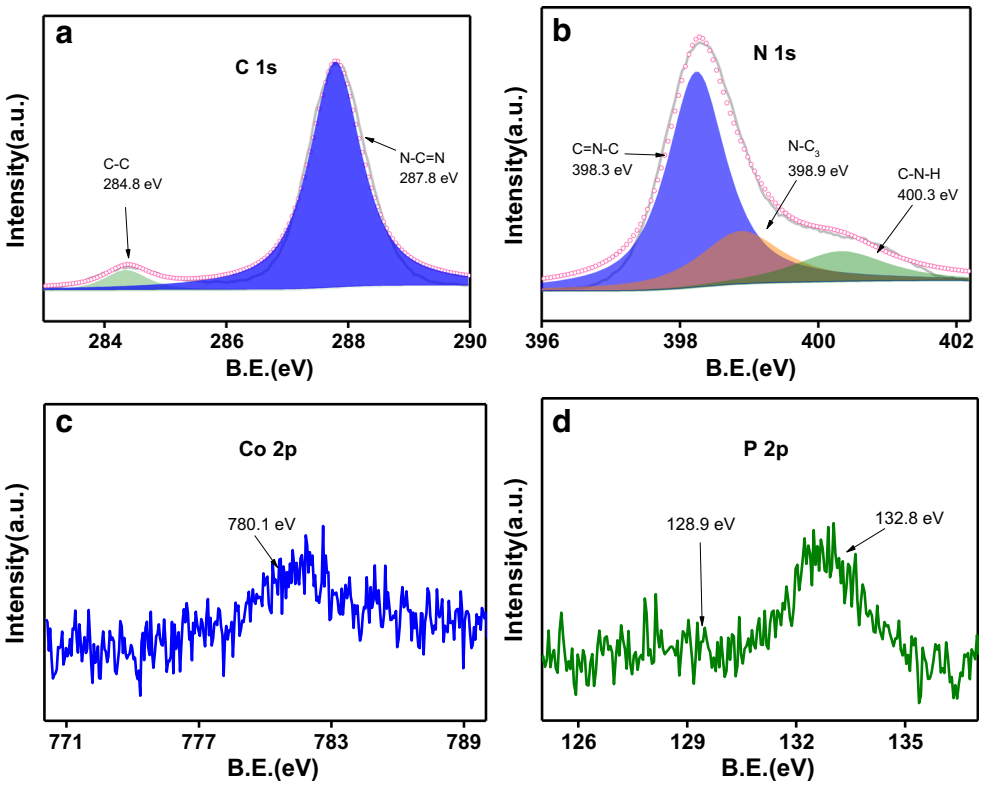

Fig. 2 For CoP/PCN (2 wt% of CoP): the high-resolution XPS spectra C1s (a), N1 s (b), Co 2p (c) and P 2p (d)

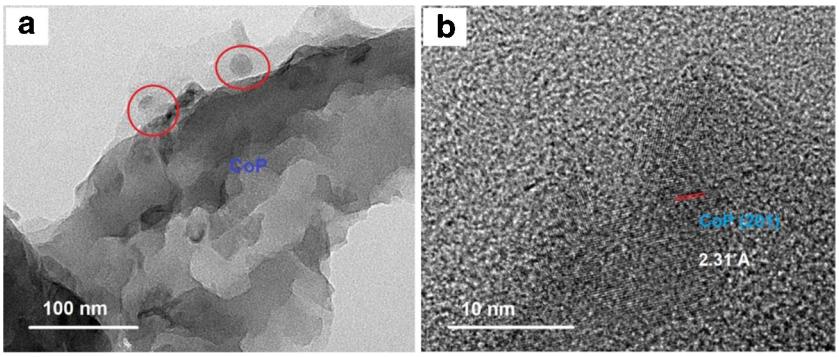

Fig. 3 **a** TEM images, **b** HRTEM image of CoP/PCN

CoP/PCN was then utilized as photoelectroactive material and supporting matrix for GO_x for fabricating the PEC glucose biosensor. According to previous reports, O_2 has been proven as electron acceptor and was found to be more efficient than H_2O_2 during the PEC process [34]. For our PEC glucose biosensor (Fig. 4c), under visible light irradiation, the photoinduced electrons from PCN will transfer to the conduction band of CoP, and then consumed by dissolved O_2 which accelerate the separation of photo-generated charges [18]. After the introduction of glucose, dissolved O_2 is reduced to H_2O_2 during the GO_x-induced enzymatic catalyzation of glucose, which result in decrease of the O_2-dependent photocurrents. This can be confirmed from Fig. 4d. The GO_x/CoP/PCN modified electrode exhibits high cathodic photocurrent (3.58 μA) in air-saturated buffer (Fig. 4d). After bubbling nitrogen to remove O_2, the photocurrent of GO_x/CoP/PCN is significantly declined, which further confirms O_2 can be used as an electron acceptor. Nevertheless, after the introduction of 500 μM H_2O_2 into the nitrogen saturated buffer, the cathodic photocurrent is increased from 0.20 μA to 1.16 μA. This result confirms the more critical effect of O_2 in this PEC process compared to H_2O_2. For glucose detection, after

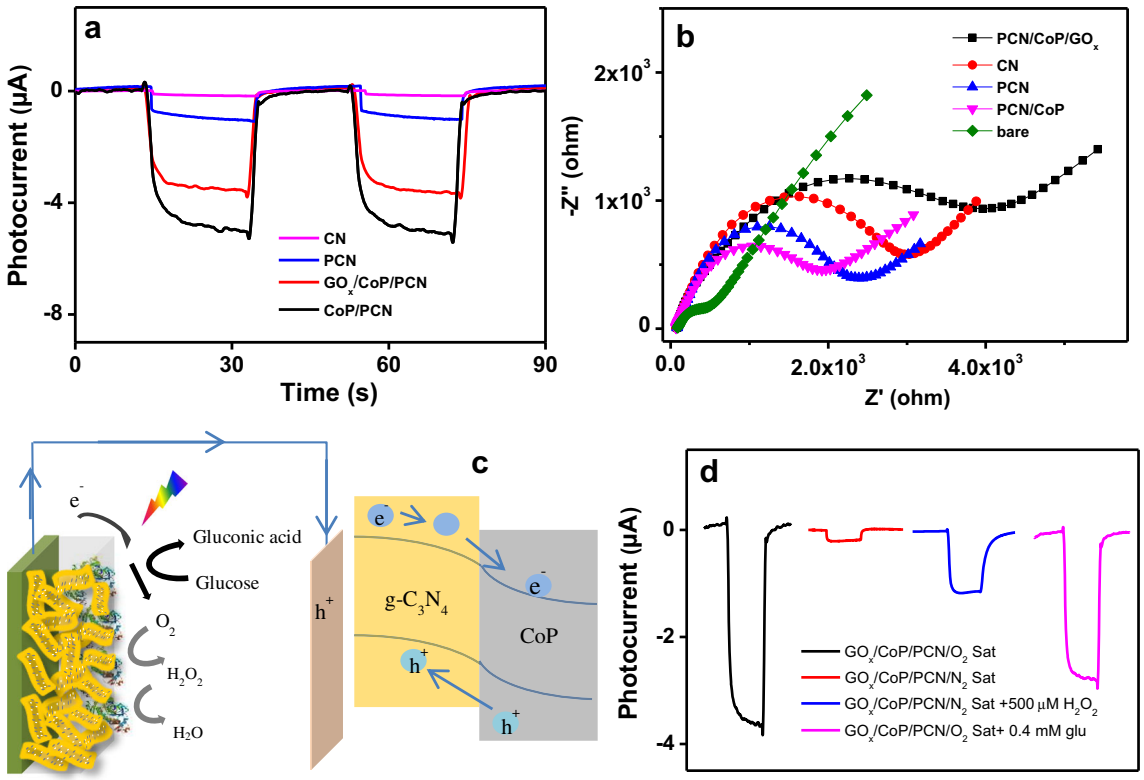

Fig. 4 **a** Photocurrent responses of different materials in PB (pH 7.4, 10 mM) at an applied potential of −0.2 V vs. Ag/AgCl. **b** Nyquist plots of materials in 5.0 mM $[Fe(CN)_6]^{3-/4-}$ containing 0.1 M KCl. **c** Mechanism of the PEC biosensor for detection of glucose. **d** Photocurrent responses of GO_x/CoP/PCN biosensor in air-saturation solution, N_2-saturation solution, N_2-saturation solution with 400 μM H_2O_2 and air-saturation solution with 0.5 mM glucose

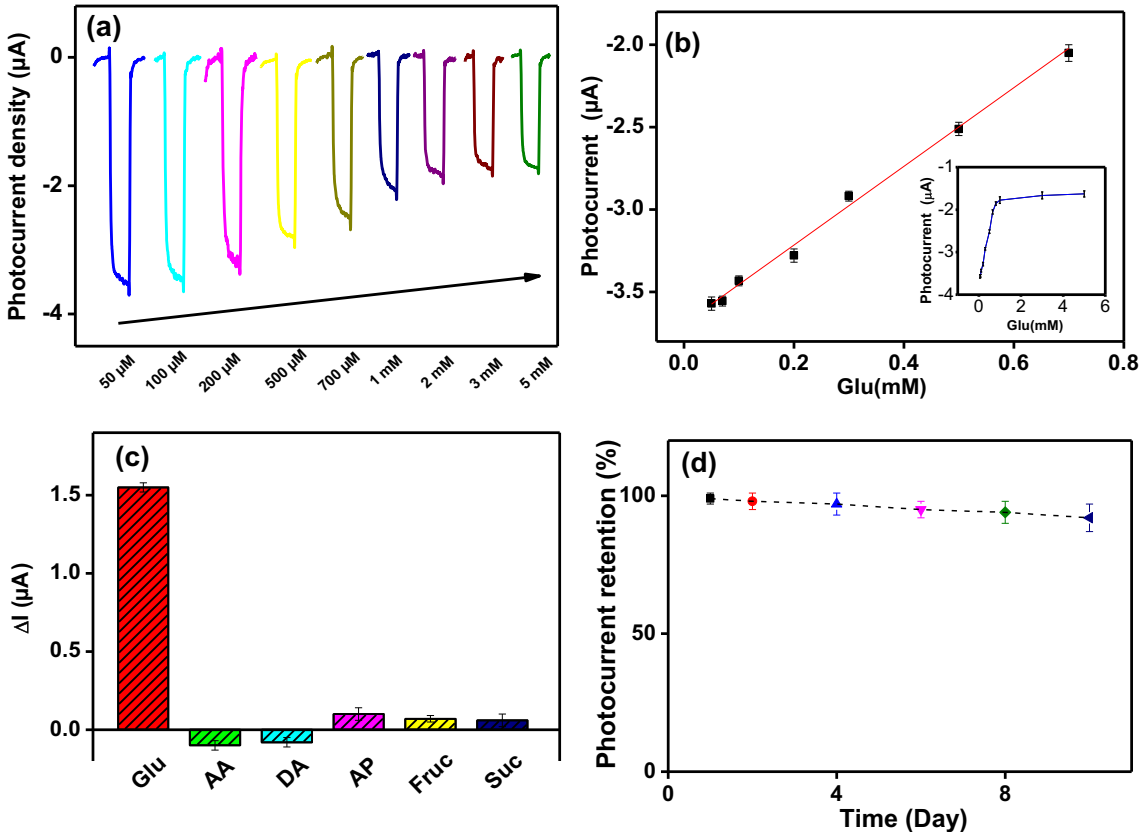

Fig. 5 **a** Photocurrent responses of the biosensor towards different concentrations of glucose. **b** Plot of the photocurrent increase with the glucose concentration. **c** Photocurrent response of the biosensor towards 1 mM glucose and 0.1 mM other interferents. **d** Stability test (over 10 days) of the biosensor

adding 0.4 mM glucose into air-saturated buffer, the photocurrent decreases to about 2.72 μA. In this way, the detection of glucose can be achieved.

The photocurrent change of the GO_x/CoP/PCN biosensor in the presence of different concentrations of glucose is depicted in Fig. 5a. With the increase of the glucose concentration, the cathodic photocurrent intensity declined accordingly. As shown in Fig. 5b, the decrease of photocurrent intensity is proportional to the glucose concentration from 0.05 to 0.7 mM.

The limit of detection is calculated to be 1.1 μM based on $S/N = 3$. In addition, compared to the performance of several other glucose sensors, this biosensor exhibits better analytical performance in term of wider linear range and lower detection limit, as shown in Table 1. The good performance of the GO_x/CoP/PCN biosensor can be ascribed to the good properties of CoP/PCN. This is primarily because (1) CoP acts as the good photosensitizer to raise the visible light adsorption efficiency [18] and (2) CoP serve as the electron acceptors from PCN to

Table 1 Analytical performance of several relevant PEC biosensors

	Detection limit	Linear range	Ref
$GO_x/Ag_2S/SnO_2$/ITO	0.032 mM	0.1–12.2 mM	[34]
GO_x/g-C_3N_4-TiO_2/ITO	0.01 mM	0.05–16 mM	[16]
BiOI/NiO/ITO	1.6 μM	0.005–10 mM	[35]
a-MoS_x/RGO/ITO	0.098 mM	0.15–16 mM	[36]
GO_x/MoS_2-TiO_2/ITO	0.015 mM	0.1–10 mM	[37]
TiO_2(G)NW@PAPBA-Au HJNH	0.11 mM	0.5–28 mM	[38]
GOD_x/NDC-TiO_2NPs/ITO	13 nM	0.05–10 μM	[39]
Au/CuS/TiO_2	30 nM	0.1–3.0 μM	[40]
TiO_2/Co_3O_4/CNT-GO_x/ITO	0.16 μM	0–4 mM	[41]
GO_x/CoP/PCN	1.1 μM	0.05–0.7 mM	This work

Table 2 Determination of glucose in 10% diluted human serum samples

Samples	Concentration measured by hospital (mM)	10% diluted human serum samples (mM)	Spiked (mM)	Measured (mM)	Recovery (%)	RSD ($n = 3$, %)
1	4.6	0.46	0.05	0.50	96.15	4.38
2	4.6	0.46	0.10	0.54	98.18	3.46
3	4.6	0.46	0.15	0.58	95.08	5.67

accelerate the photoinduced charges separation, which means photoinduced electrons (e^-) of PCN can be easily migrated to CoP, while the holes (h^+) tended to transfer from CoP to PCN, resulting in improvement of the PEC response [27].

For accurate detection of glucose in real samples, such as in blood sample, it is important to eliminate various interfering substances. These species include ascorbic acid (AA), uric acid (UA), and acetaminophen (AP). Since in physiological condition, the concentration of glucose (3–8 mM) is much higher than the concentration of these species (<0.5 mM), the response of the electrode to 1 mM glucose, 0.1 mM AA and AP were studied. As shown in Fig. 5c, besides these interfering substances, fructose (Fruc) and sucrose (Suc) also have no obvious effect on the photocurrent responses of the biosensor. As for the reason, the inherent specificity of the enzyme and low detection potential avoids detection interferences. In Fig. S6, the biosensor displayed excellent reproducibility. Furthermore, the long-term durability of this PEC biosensor was investigated. As shown in Fig. 5d, the photocurrent is stable and only slightly decays observed after 15 days of storage.

The feasibility of the biosensor for practical application was assessed by analyzing glucose in diluted serum samples [42, 43]. As shown in Table 2, the initial concentration of glucose in the serum sample was determined and then different concentrations of glucose were added into the sample. Recovery results between 95.08~98.18% are obtained, indicating that the glucose biosensor can be utilized for human serum sample analysis.

From the above data, the good stability, high sensitivity and wide analytical range of the GO_x/CoP/PCN biosensor shows good potential to be applied in the biomedical, health care, food industry and environmental areas for glucose detection. However, as an enzyme-based glucose sensor, several drawbacks need to be overcome, such as restricted operational conditions. Therefore, our next research direction will be for the construction of the non-enzymatic PEC sensors for glucose detection.

Conclusions

We have successfully prepared PEC glucose biosensor based on CoP/PCN nanocomposites synthesized by a thermal phosphating process and subsequently functionalized with glucose oxidase. The CoP/PCN exhibited high PEC response under visible light illumination compared to CN and PCN, which can be attributed to the improvement of the photoinduced charge separation in CoP. In the presence of glucose, O_2-dependent suppression of the photocurrent was clearly observed in biosensor. As a result, the GO_x/CoP/PCN biosensor displayed good performances for glucose detection and also realized the determination of glucose in diluted human serum samples. Overall, wide analytical range, low detection limit and good selectivity indicate wide potential to be applied in different areas for glucose analysis.

Acknowledgments This work was supported by the Natural Science Foundation of Hunan Province (2017JJ2326).

References

1. Ye C, Wang MQ, Luo HQ, Li NB (2017) Label-free photoelectrochemical "off-on" platform coupled with G-wire-enhanced strategy for highly sensitive microRNA sensing in cancer cells. Anal Chem 89:11697–11702. https://doi.org/10.1021/acs.analchem.7b03150
2. Zhao WW, Xu JJ, Chen HY (2014) Photoelectrochemical DNA biosensors. Chem Rev 114:7421–7441. https://doi.org/10.1021/cr500100j
3. Li M, Xiong C, Zheng Y, Liang W, Yuan R, Chai Y (2018) Ultrasensitive photoelectrochemical biosensor based on DNA tetrahedron as nanocarrier for efficient immobilization of CdTe QDs-methylene blue as signal probe with near-zero background noise. Anal Chem 90:8211–8216. https://doi.org/10.1021/acs.analchem.8b01641
4. Deng D, Hao Y, Yang S, Han Q, Liu L, Xiang Y, Tu F, Xia N (2019) A signal-on electrochemical biosensor for evaluation of caspase-3 activity and cell apoptosis by the generation of molecular electrocatalysts on graphene electrode surface for water oxidation. Sensors Actuators B Chem 286:415–420. https://doi.org/10.1016/j.snb.2019.01.137
5. Liu L, Deng D, Wang Y, Song K, Shang Z, Wang Q, Xia N, Zhang B (2018) A colorimetric strategy for assay of protease activity based on gold nanoparticle growth controlled by ascorbic acid and cu(II)-coordinated peptide. Sensors Actuators B Chem 266:246–254. https://doi.org/10.1016/j.snb.2018.03.116
6. Tang J, Zhang Y, Kong B, Wang Y, Da P, Li J, Elzatahry AA, Zhao D, Gong X, Zheng G (2014) Solar-driven photoelectrochemical probing of nanodot/nanowire/cell interface. Nano Lett 14:2702–2708. https://doi.org/10.1021/nl500608w

7. Gill R, Zayats M, Willner I (2008) Semiconductor quantum dots for bioanalysis. Angew Chem Int Ed 47:7602–7625. https://doi.org/10.1002/anie.200800169
8. Shu J, Qiu Z, Lv S, Zhang K, Tang D (2018) Plasmonic enhancement coupling with defect-engineered TiO_2-x: a mode for sensitive photoelectrochemical biosensing. Anal Chem 90:2425–2429. https://doi.org/10.1021/acs.analchem.7b05296
9. Muthuchamy N, Lee KP, Gopalan AI (2017) Enhanced photoelectrochemical biosensing performances for graphene (2D)-titanium dioxide nanowire (1D) heterojunction polymer conductive nanosponges. Biosens Bioelectron 89:390–399. https://doi.org/10.1016/j.bios.2016.06.005
10. Low J, Dai B, Tong T, Jiang C, Yu J (2019) In situ irradiated x-ray photoelectron spectroscopy investigation on a direct Z-scheme TiO_2/CdS composite film photocatalyst. Adv Mater 31:1802981–1802985. https://doi.org/10.1002/adma.201802981
11. Yan Z, Wang Z, Miao Z, Liu Y (2016) Dye-sensitized and localized surface plasmon resonance enhanced visible-light photoelectrochemical biosensors for highly sensitive analysis of protein kinase activity. Anal Chem 88:922–929. https://doi.org/10.1021/acs.analchem.5b03661
12. Wang S, Li S, Wang W, Zhao M, Liu J, Feng H, Chen Y, Gu Q, Du Y, Hao W (2019) A non-enzymatic photoelectrochemical glucose sensor based on $BiVO_4$ electrode under visible light. Sensors Actuators B Chem 291:34–41. https://doi.org/10.1016/j.snb.2019.04.057
13. Wang K, Sun N, Li XP, Zhang RH, Zu GY, Wang J, Pei RJ (2015) A hemin binding G-quadruplex/Pb^{2+} complex to construct a visible light activated photoelectrochemical sensor on a ZnO/BiOI heterostructure. Anal Methods 7:9340–9346. https://doi.org/10.1039/C5AY02197A
14. Haddour N, Chauvin J, Gondran C, Cosnie S (2006) Photoelectrochemical immunosensor for label-free detection and quantification of anti-cholera toxin antibody. J Am Chem Soc 128:9693–9698
15. Yin H, Zhou Y, Li B, Li X, Yang Z, Ai S, Zhang X (2016) Photoelectrochemical immunosensor for microRNA detection based on gold nanoparticles-functionalized g-C_3N_4 and anti-DNA:RNA antibody. Sensors Actuators B Chem 222:1119–1126. https://doi.org/10.1016/j.snb.2015.08.019
16. Liu P, Huo X, Tang Y, Xu J, Liu X, Wong DKY (2017) A TiO_2 nanosheet-g-C_3N_4 composite photoelectrochemical enzyme biosensor excitable by visible irradiation. Anal Chim Acta 984:86–95. https://doi.org/10.1016/j.aca.2017.06.043
17. Sun ZJ, Lv B, Li JS, Xiao M, Wang XY, Du PW (2016) Core–shell amorphous cobalt phosphide/cadmium sulfide semiconductor nanorods for exceptional photocatalytic hydrogen production under visible light. J Mater Chem A 4:1598–1602. https://doi.org/10.1039/C5TA07561K
18. Tian J, Zhu H, Chen J, Zheng X, Duan H, Pu K, Chen P (2017) Cobalt phosphide double-shelled nanocages: broadband light-harvesting nanostructures for efficient photothermal therapy and self-powered photoelectrochemical biosensing. Small 13:1700798. https://doi.org/10.1002/smll.201700798
19. Xia L, Song J, Xu R, Liu D, Dong B, Xu L, Song H (2014) Zinc oxide inverse opal electrodes modified by glucose oxidase for electrochemical and photoelectrochemical biosensor. Biosens Bioelectron 59:350–357. https://doi.org/10.1016/j.bios.2014.03.038
20. Chen D, Jiang D, Du X, Zhou L, Huang L, Qian J, Liu Q, Hao N, Li Y, Wang K (2016) Engineering efficient charge transfer based on ultrathin graphite-like carbon nitride/WO_3 semiconductor nanoheterostructures for fabrication of high-performances non-enzymatic photoelectrochemical glucose sensor. Electrochim Acta 215:305–312. https://doi.org/10.1016/j.electacta.2016.08.113
21. Zeng K, Yang MH, Liu YN, Rasooly A (2018) Dual function hollow structured mesoporous Prussian blue mesocrystals for glucose biosensors. Anal Methods 10:3951–3957. https://doi.org/10.1039/c8ay01456f
22. Çakıroğlu B, Demirci YC, Gökgöz E, Özacar M (2019) A photoelectrochemical glucose and lactose biosensor consisting of gold nanoparticles, MnO_2 and g-C_3N_4 decorated TiO_2. Sensors Actuators B Chem 282:282–289. https://doi.org/10.1016/j.snb.2018.11.064
23. Vashist SK (2012) Non-invasive glucose monitoring technology in diabetes management: a review. Anal Chim Acta 750:16–27. https://doi.org/10.1016/j.aca.2012.03.043
24. Liang D, Huang Y, Wu F, Luo J, Yi X, Wang J, Qiu X (2019) In situ synthesis of g-C_3N_4/TiO_2 with {001} and {101} facets coexposed for water remediation. Appl Surf Sci 487:322–334. https://doi.org/10.1016/j.apsusc.2019.05.088
25. Xiao T, Tang Z, Yang Y, Tang L, Zhou Y, Zou Z (2018) In situ construction of hierarchical WO_3/g-C_3N_4 composite hollow microspheres as a Z-scheme photocatalyst for the degradation of antibiotics. Appl Catal B Environ 220:417–428. https://doi.org/10.1016/j.apcatb.2017.08.070
26. Nie H, Ou M, Zhong Q, Zhang S, Yu L (2015) Efficient visible-light photocatalytic oxidation of gaseous NO with graphitic carbon nitride (g-C_3N_4) activated by the alkaline hydrothermal treatment and mechanism analysis. J Hazard Mater 300:598–606. https://doi.org/10.1016/j.jhazmat.2015.07.066
27. Yi SS, Yan JM, Wulan B, Li S, Liu K, Jiang Q (2017) Noble-metal-free cobalt phosphide modified carbon nitride: an efficient photocatalyst for hydrogen generation. Appl Catal B Environ 200:477–483. https://doi.org/10.1016/j.apcatb.2016.07.046
28. Yang P, Wang R, Zhou M, Wang X (2018) Photochemical construction of carbonitride structures for red-light redox catalysis. Angew Chem Int Ed 57:1–5. https://doi.org/10.1002/anie.201804996
29. Li YX, Ouyang SX, Xu H, Wang X, Bi YP, Zhang YF, Ye JH (2016) Constructing solid-gas-interfacial Fenton reaction over alkalinized-C_3N_4 photocatalyst to achieve apparent quantum yield of 49% at 420 nm. J Am Chem Soc 138:13289–13297. https://doi.org/10.1021/jacs.6b07272
30. Zhang S, Li J, Wang X, Huang Y, Zeng M, Xu J (2014) In situ ion exchange synthesis of strongly coupled Ag@AgCl/g-C_3N_4 porous nanosheets as plasmonic photocatalyst for highly efficient visible-light photocatalysis. ACS Appl Mater Interfaces 6:22116–22125. https://doi.org/10.1021/am505528c
31. Wang GL, Liu KL, Dong YM, Wu XM, Li ZJ, Zhang C (2014) A new approach to light up the application of semiconductor nanomaterials for photoelectrochemical biosensors: using self-operating photocathode as a highly selective enzyme sensor. Biosens Bioelectron 62:66–72. https://doi.org/10.1016/j.bios.2014.06.033
32. Zhang YH, Tang ZR, Fu XZ, Xu YJ (2011) Engineering the unique 2D mat of graphene to achieve graphene-TiO_2 nanocomposite for photocatalytic selective transformation: what advantage does graphene have over its forebear carbon nanotube? ACS Nano 9:7426–7435
33. Peng GM, Xing LD, Barrio J, Volokh M, Shalom M (2018) A general synthesis of porous carbon nitride films with tunable surface area and photophysical properties. Angew Chem Int Ed 57:1186–1192. https://doi.org/10.1002/anie.201711669
34. Zhang X, Liu M, Liu H, Zhang S (2014) Low-toxic Ag_2S quantum dots for photoelectrochemical detection glucose and cancer cells. Biosens Bioelectron 56:307–312. https://doi.org/10.1016/j.bios.2014.01.033
35. Zhang L, Ruan YF, Liang YY, Zhao WW, Yu XD, Xu JJ, Chen HY (2018) Bismuth Oxyiodide couples with glucose oxidase: a special synergized dual-catalysis mechanism for Photoelectrochemical

enzymatic bioanalysis. ACS Appl Mater Interfaces 10(4):3372–3379. https://doi.org/10.1021/acsami.7b17647

36. Shang M, Qi H, Du C, Huang H, Wu S, Zhang J, Song W (2018) One-step electrodeposition of high-quality amorphous molybdenum sulfide/RGO photoanode for visible-light sensitive photoelectrochemical biosensing. Sensors Actuators B Chem 266:71–79. https://doi.org/10.1016/j.snb.2018.03.117
37. Liu X, Huo X, Liu P, Tang Y, Xu J, Liu X, Zhou Y (2017) Assembly of MoS_2 nanosheet-TiO_2 nanorod heterostructure as sensor scaffold for photoelectrochemical biosensing. Electrochim Acta 242:327–336. https://doi.org/10.1016/j.electacta.2017.05.037
38. Nallal M, Anantha Iyengar G, PillLee K (2017) New titanium dioxide-based heterojunction nanohybrid for highly selective photoelectrochemical-electrochemical dual-mode sensors. ACS Appl Mater Interfaces 9:37166–37183. https://doi.org/10.1021/acsami.7b10519
39. Atchudan R, Muthuchamy N, Edison T, Perumal S, Vinodh R, Park KH, Lee YR (2019) An ultrasensitive photoelectrochemical biosensor for glucose based on bio-derived nitrogen-doped carbon sheets wrapped titanium dioxide nanoparticles. Biosens Bioelectron 126:160–169. https://doi.org/10.1016/j.bios.2018.10.049
40. Wang Y, Bai L, Wang Y, Qin D, Shan D, Lu X (2018) Ternary nanocomposites of au/CuS/TiO_2 for an ultrasensitive photoelectrochemical non-enzymatic glucose sensor. Analyst 143(7):1699–1704. https://doi.org/10.1039/c8an00187a
41. Cakiroglu B, Ozacar M (2018) A self-powered photoelectrochemical glucose biosensor based on supercapacitor Co_3O_4-CNT hybrid on TiO_2. Biosens Bioelectron 119:34–41. https://doi.org/10.1016/j.bios.2018.07.049
42. Guo Q, Liu L, Zhang M, Hou H, Song Y, Wang H, Zhong B, Wang L (2017) Hierarchically mesostructured porous TiO_2 hollow nanofibers for high performance glucose biosensing. Biosens Bioelectron 92:654–660. https://doi.org/10.1016/j.bios.2016.10.036
43. Shrestha BK, Ahmad R, Mousa HM, Kim IG, Kim JI, Neupane MP, Park CH, Kim CS (2016) High-performance glucose biosensor based on chitosan-glucose oxidase immobilized polypyrrole/Nafion/functionalized multi-walled carbon nanotubes bio-nanohybrid film. J Colloid Interface Sci 482:39–47. https://doi.org/10.1016/j.jcis.2016.07.067